Available online at www.sciencedirect.com

ScienceDirect

Proceedings of the Combustion Institute 38 (2021) 345–353

Proceedings of the Combustion Institute

www.elsevier.com/locate/proci

Ammonia–methane interaction in jet-stirred and flow reactors: An experimental and kinetic modeling study

Suphaporn Arunthanayothin [a], Alessandro Stagni [b], Yu Song [a,c], Olivier Herbinet [a,*], Tiziano Faravelli [b], Frédérique Battin-Leclerc [a]

[a] *Université de Lorraine, CNRS, LRGP, F-54000 Nancy, France*
[b] *CRECK Modeling Lab, Department of Chemistry, Materials and Chemical Engineering "G. Natta", Politecnico di Milano, P.zza Leonardo da Vinci 32, 20133 Milano, Italy*
[c] *Laboratoire PRISME, Université d'Orléans, Polytech Vinci, 45072 Orléans cedex, France*

Received 7 November 2019; accepted 2 July 2020
Available online 18 September 2020

Abstract

The influence of the addition of ammonia on the oxidation of methane was investigated both experimentally and numerically. Experiments were carried out at atmospheric pressure, using a fused silica jet-stirred reactor, and a recrystallized alumina tubular reactor designed on purpose to reach temperatures as high as ~2000 K. A temperature range of 600–1200 K was investigated in the jet-stirred reactor at a residence time of 1.5 s, while experiments in the flow reactor were carried out between 1200 and 2000 K, for a fixed residence time of about 25 ms in the reactive zone. A methane/ammonia mixture, diluted in helium, was used in both reactors with equivalence ratios varied between 0.5 and 2 in the first reactor, while stoichiometric conditions were investigated in the second one. The measurements indicate that CH_4 reactivity was promoted by NH_3 addition below 1200 K, but not so much influenced above. These results were interpreted and explained using a comprehensive kinetic model, previously validated over a wider range of operating conditions. The mechanism allowed to shed light on the underlying causes of the anticipated methane reactivity at low temperature, and of the major role played by NO_x in it. This effect was shown to become less significant at higher temperatures, where the reactivity is mainly governed by H-abstractions on both fuels.

Keywords: Ammonia; Jet-stirred reactor; Flow reactor; Oxidation; Detailed kinetic modeling

1. Introduction

Nowadays, a great attention is being paid to the gas-phase oxidation of ammonia, either as pure or mixed with other hydrocarbons. Ammonia is one of the components of biogas, a potentially renewable fuel produced via the anaerobic diges-

* Corresponding author.
E-mail address: olivier.herbinet@univ-lorraine.fr (O. Herbinet).

https://doi.org/10.1016/j.proci.2020.07.061

tion of organic feedstocks. Biogas is primarily composed of methane and carbon dioxide, with smaller amounts of water, nitrogen, oxygen, ammonia and hydrogen sulfide. Its relative composition varies according to the original source [1,2], which may have an influence on the reactivity and the pollutant formation when biogas is used as a fuel. In addition, ammonia is a potentially carbon-free fuel, which could be used, like hydrogen, as a flexible energy carrier, with applications in several industrial sectors [3]. Therefore, it has the potential to store excess energy, and unlock the vast potential of intermittent renewable energy (e.g. wind, sun [4]). Due to its weak combustion properties, co-firing of ammonia with a combustion enhancer (e.g. hydrogen, methane or coal) is one of the proposed solutions to allow its use in gas turbines, engines or industrial furnaces [3,5,6]. Whatever the application domain, a comprehensive understanding of ammonia combustion characteristics and its mutual interaction with species like methane is essential for designing efficient industrial processes and controlling undesired emissions. Indeed, the presence of nitrogen in the molecule makes ammonia kinetics intrinsically related to the formation of Nitrogen Oxides (NO_x), either as fuel or intermediate species (e.g. organic fuels containing nitrogen).

The literature is very rich in experimental data for neat methane and neat ammonia [7], but much less is available with regard to the oxidation of ammonia–methane mixtures, in spite of the growing interest. Most of ammonia–methane oxidation studies were performed in premixed flames (e.g., [8,9]) with a focus on the detection of flame intermediates [10–12], or on the measurements of adiabatic burning velocities [13,14]. Previous studies were also carried out in flow reactors [15,16] where the oxidation of NH_3/CH_4 mixtures in N_2 or CO_2 environments was investigated, at atmospheric pressure and intermediate/high-temperatures with NO, CO and CO_2 quantification. Other studies on the oxidation of methane doped with ammonia using CO_2 as bath gas were performed in flames [8,17–19]. Several detailed kinetic models were proposed to account for the oxidation chemistry of ammonia/methane mixtures, and to investigate the mutual interaction between the two fuels [8,15,20,21].

In order to better understand ammonia–methane interaction in a wider range of operating temperature conditions, we performed experimental campaigns using two different configurations, respectively a Jet-Stirred Reactor (JSR) and a Flow Reactor (FR), such as to cover low-, intermediate- and high-temperature conditions. A detailed analysis of reaction products and intermediates was performed, and the results were interpreted with a comprehensive kinetic model, developed through a first-principles approach, describing the oxidation of methane and ammonia, as well as both fuel interaction and NO_x formation.

2. Experimental methodology

The co-oxidation of methane and ammonia was experimentally investigated using two different reactors (see additional details in Supplementary Material (SM1)) working close to atmospheric pressure, with helium as carrier gas. Mass flow controllers were used for reactor feeding (relative uncertainty of ±0.5% in flow). In a first set-up, experiments were performed in a fused silica JSR, a type of continuous stirred-tank reactor usually operated at steady state. JSRs were used for several gas-phase kinetic studies and the present JSR setup was already described in previous works [22–24]. It consisted of a spherical vessel with injection of the fresh mixture through four nozzles located at the center of the reactor, creating high turbulence resulting in homogeneity in composition and temperature. As a result, the JSR can be modeled as a perfectly stirred reactor. Its residence time was fixed at 1.5 s. The heating of the reactor was achieved though Inconel resistances, and the reaction temperature was measured with a K-type thermocouple located in a glass finger close to the center of the reactor (uncertainty of ±5 K).

A second setup was used to investigate the co-oxidation of CH_4 and NH_3 at higher temperature (up to ∼2000 K) in a flow reactor (FR), consisting in an alumina tube (inner diameter of 4 mm and 100 cm in length) designed to approximate plug flow conditions with the Peclet numbers >50 (see SM1). The reactor was located horizontally in an electrically heated oven (Carbolite Gero). Temperature profiles were measured with a R-type thermocouple (profiles are provided in SM2). The isothermal reaction zone is located between 36 and 58 cm with a uniform temperature profile (± 30 K). For each experiment, the residence time was fixed to about 25 ms in the central zone where the temperature can be considered constant. It must be noted that undesirable catalytic effects of the reactor wall were first observed in FR when using non recrystallized alumina.

The reactants and reaction products were analyzed using four diagnostics:

- Two gas chromatographs (GCs) were used for the quantification of carbon-containing species such as methane, carbon monoxide, carbon dioxide and the three C_2 hydrocarbons (the carrier gas was helium). They were equipped with GSQ (JSR setup) and PlotQ (FR setup) capillary columns, respectively. Both included a Flame Ionization Detector (FID) preceded by a methanizer (for the reduction by H_2 of oxygenated and nitrogenated functional groups over a heated nickel catalyst) allowing a better sensitivity for CO, CO_2 and HCN detection than a thermal conductivity detector. Calibrations were performed using gaseous standards or using

the "effective carbon number" method for carbon containing species [24].

- Nitric oxide (NO) and nitrogen dioxide (NO_2) were detected in JSR and FR experiments using a dedicated NO_x analyzer (Thermo Scientific Model 42i), based on chemiluminescence. This analyzer had two channels, one for the detection of nitric oxide in a direct and independent way, and a second one for the measure of the total NO_x concentration. Calibrations were performed using gaseous standards.
- A continuous-wave Cavity Ring-Down Spectroscopy (cw-CRDS) cell coupled to the JSR by a sonic probe was used for ammonia quantification. This technique was previously successfully used for the detection of species, such as hydrogen peroxide during the oxidation of alkanes [25] and HONO during the oxidation of *n*-pentane doped with nitric oxide [26]. Ammonia has strong absorption lines in the wavelength range 6637–6643 cm^{-1}, making the quantification accurate and providing a good sensibility. Cross sections were deduced from data recorded under non-reactive conditions.
- On-line mass-spectrometry was used to detect NH_3, N_2, H_2O, CH_4, CO_2 and O_2 during the co-oxidation of CH_4 and NH_3 in FR. Sampling was achieved through a capillary tube directly connecting the FR outlet and the analyzer. This technique requires the calibration of each species as there is no obvious relationship between their structures and their calibration factors. Gaseous standards were used except for CO_2 and water, which were calibrated considering the reaction complete at the highest temperature.
- Fourier Transform InfraRed Spectroscopy was used to highlight the possible presence of N_2O as this species has a strong absorption in the 400–4000 cm^{-1} wavelength range. However, no N_2O was observed during experiments, likely due to concentrations below the detection limit (estimated to 50 ppm at 2237.5 cm^{-1}).

Relative uncertainties in mole fractions are ±5% for species detected by gas chromatography and NO. It is ±10% for ammonia quantified by CRDS, NO_2 and the species detected by online mass spectrometry.

3. Kinetic model

The kinetic model describing ammonia and methane oxidation and their mutual interaction was obtained by following a hierarchical methodology, i.e. the founding principle of the CRECK framework [27]. The mechanism relied on a core C_0–C_2 module developed by Metcalfe et al. [28], on top of which the C_3 mechanism of Burke et al. [29] was added. Thermodynamic properties were taken from the database of Burcat and Ruscic [30].

NO_x submechanism leveraged the recent work of Song et al. [22], where its capability to represent the sensitizing effects of both NO and NO_2 on CH_4 oxidation at lower temperatures had been demonstrated. This served as a basis for the development of this new ammonia oxidation mechanism, which was performed via an *ab-initio* evaluation of the ammonia decomposition and H-abstraction reactions. A full description of the mechanism construction and its wide-range validation can be found in the paper by Stagni et al. [7].

The complete mechanism is made up of 157 species and 2444 reactions, and is available under CHEMKIN format in SM3-5, along with thermodynamic and transport properties. For the sake of completeness, a wide-range validation in the conditions of interest is also reported in Fig. S4–S12 in SM1.

4. Experimental results

In this work, the equivalence ratio (Φ) was defined considering CO_2, water and NO as final combustion products from methane and ammonia oxidation. NO was considered rather than N_2, since non-negligible amounts of NO were formed under the conditions of this study.

4.1. Jet-stirred reactor

JSR experiments were performed over the temperature range 600–1200 K, at a residence time of 1.5 s, a pressure of 106.7 kPa, with inlet methane and ammonia mole fractions of 10,000 and 500 ppm, respectively, and at three equivalence ratios (0.5, 1 and 2). Two particular phenomena were observed during experiments, making the oxidation study of methane/ammonia mixtures tricky. The first was the occurrence of oscillation regimes under specific conditions (at the highest temperatures for the lean and stoichiometric mixtures). Mole fractions were not constant in time, which was not compatible with the diagnostics used in this study. For this reason, the investigated temperature range is limited for some conditions in the results displayed hereafter. This phenomenon has been previously reported in literature for the oxidation of neat methane [31], and its kinetic foundations were explained in [32]. The second phenomenon was the occurrence of wall reactions strongly enhancing the ammonia consumption, although the reactor was made of fused silica. This problem was solved by treating the surface of the JSR before each experiment by flowing all gases but ammonia under reactive conditions.

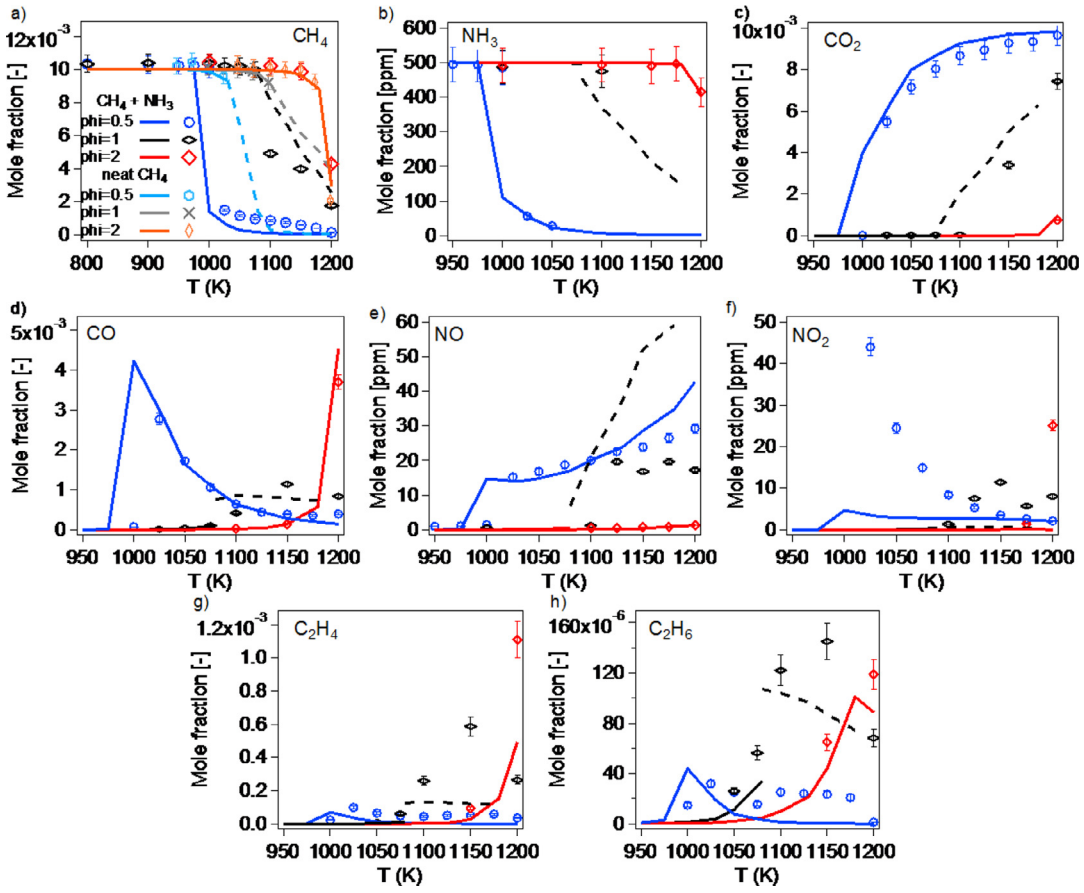

Fig. 1. Mole fractions of reactants and main reaction products at a variable temperature and equivalence ratio in the JSR. Symbols: experiments. Lines: data computed with the model (dashed lines are averaged mole fractions due to oscillation regime).

Figure 1 displays the mole fractions of both reactants and main products. The temperature of the reactivity onset is very sensitive to the equivalence ratio: it is about 1000 K for the lean condition, 1075 K for the stoichiometric ones, and 1150 K in rich mixtures, according to the temperature dependence of the methane and ammonia mole fractions shown in Fig. 1a–b. Figure 1a also displays CH_4 mole fractions in the case of the oxidation of neat methane for comparison. Mole fractions are comparable to those of methane when doped with ammonia for the rich conditions, whereas the reactivity onset is anticipated (~100 K) by ammonia addition under lean conditions, and conversion is slightly enhanced in stoichiometric conditions.

The main carbon containing products are carbon monoxide, carbon dioxide, ethylene and ethane (Fig. 1). Under lean conditions, carbon monoxide mole fractions peak at 1025 K. Above this temperature, a decrease of the CO mole fraction is observed with a simultaneous increase of that of CO_2. The mole fractions of ethylene and ethane remain low (less than 500 ppm). Larger equivalence ratios favor the formation of unburnt species.

Only two nitrogen-containing species were detected during this study: nitric oxide (NO) and nitrogen dioxide (NO_2), but more N-containing species should be formed in significant amounts because the N-atom balance is not closed. This is likely due to the formation of N_2, which was expected, but its detection was not possible because of interference in GC analyses. NO and NO_2 mole fractions are displayed in Fig. 1e–f. Under lean conditions, the mole fractions of these last products increase simultaneously to ammonia depletion. NO_2 mole fraction already peaks at 1025 K and afterward decreases whereas that of NO continue to increase. Note that NO behaves closely to CO_2 whereas NO_2 behaves closely to CO.

Under stoichiometric conditions, oscillation behavior was detected above 1025 K. Beyond this temperature, data for ammonia are not accurate

because oscillations are not compatible with the CRDS spectrum acquisition time of ammonia (about 30 min) and the in-situ sampling. Data recorded with the NO_x analyzer and by GC, with a sampling strategy based on the injection of a defined volume accumulated on the larger time scale, can be considered as time averages. Oscillations seem to have a minor impact on species like methane, carbon monoxide and carbon dioxide. This is because the mole fractions of these species are larger compared to those of nitric oxide and nitrogen dioxide.

4.2. Flow reactor

FR experiments were performed over a temperature range significantly higher than in the JSR thanks to the use of a recrystallized alumina tube and an oven heating up to temperatures as high as ~2000 K. The two fuels, the oxidizer, and 11 reaction products were followed. Reaction products can be divided as follows:

- Species specific to methane oxidation: CO, CO_2, C_2H_2, C_2H_4, C_2H_6 and C_3H_6.
- Species specific to ammonia oxidation: N_2, NO and NO_2.
- Species common to both fuels: water and HCN.

Note that HCN is the only fuel cross-product whose formation was observed during these high temperature experiments. Mole fraction profiles are displayed in Fig. 2. C-, N-, H- and O-atom balances were calculated for each temperature and are all in the range of 0.99±0.05 (see values in Table S4 in SM1).

The consumption of methane and ammonia becomes significant starting from ~1500 K and they are already totally consumed at ~1600 K. The two main products from the oxidation of methane are CO and CO_2. CO peaks at 1573 K and is then progressively converted to CO_2 when the temperature increases. Ammonia is mainly converted to NO and N_2, and NO/N_2 ratio slightly increases with temperature. Note that under these conditions, equilibrium calculations predict the formation of N_2 quasi exclusively. Small amounts of NO_2 were also observed on a very narrow range (between 1550 and 1600 K). A part of O_2 remains not consumed even at the highest temperatures because of the formation of N_2 from NH_3 (the NH_3/O_2 inlet ratio was calculated considering only NO as product to be sure to have enough oxygen for fully consuming methane). Other reaction products (C_2 species, C_3H_6 and HCN) are produced in small amounts and over a narrow temperature range as for NO_2 (Fig. 2e).

5. Comparison between experimental and simulated results

Figures 1 and 2 compare the experimental data and model results. The kinetic model well predicts the temperature of the reactivity onset for both reactors as it can be seen for methane and ammonia in Figs. 1 and 2. The temperature dependence of the conversion of both fuels is also well predicted, although the residual presence of methane after $T = 1025$ K is underestimated. In the JSR, at Φ=1, where oscillation behavior was detected above 1025 K, the mole fractions of methane (GC detection) reasonably agree with averaged computed mole fractions (dashed lines in Fig. 1). The model predicts the anticipated reactivity of methane in presence of ammonia under lean conditions.

As far as JSR reaction products are concerned, mole fractions of carbon monoxide and of carbon dioxide are well predicted by the model at all equivalence ratios (even for the stoichiometric case for which oscillating computed mole fractions were averaged). Mole fractions of ethane and NO are also reproduced fairly well by the model. Discrepancies are observed for nitrogen dioxide for which the model under-estimates the formation, especially under lean conditions. This issue was also previously observed by Song et al. in the CH_4 oxidation doped with NO [22]. For the rich case, the signal detected for NO_2 under these high temperature conditions is likely due to an interference with that of HCN, which is a typical high temperature product under rich conditions (whereas NO_2 is usually produced at low-temperature oxidation), as already observed in [22].

In the FR, the agreement is also quite satisfactory for the main reaction products such as water, NO and N_2. Surprisingly, the model predicts a more abrupt increase of CO_2 and decrease of CO mole fractions than in the experiments. This trend is also observed when studying the oxidation of neat methane (open symbols in Fig. 2a), indicating that it is not due to the presence of ammonia in the feed of the reactor. According to a kinetic analysis performed at 1600 K, the second most sensitive reaction is CO+OH=CO_2+H (after the branching reaction H + O_2=OH+O) the kinetic parameters of which are relatively well known. With the current mechanism there is no way to explain this deviation, as well as the pre-reaction of NH_3 before ignition (which was also observed in [15] with different inlet mixtures). The model predicts negligible amounts of NO_2, C_3H_6 and HCN compared to the experiment.

6. Kinetic analysis

Rate-of-production and sensitivity analyses were performed to highlight the chemistry involved

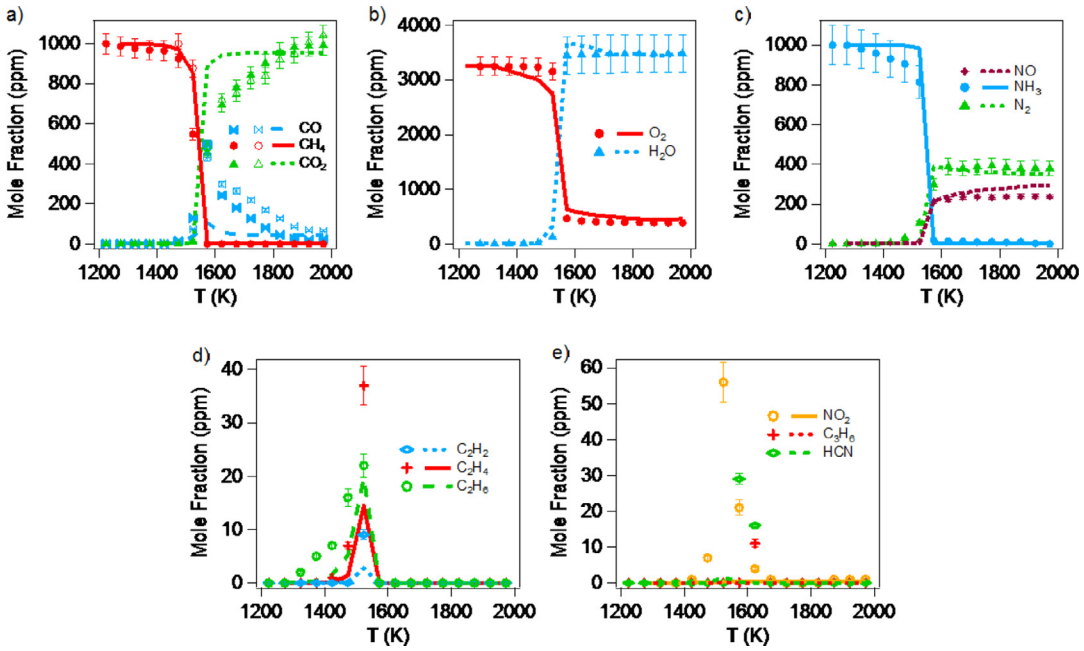

Fig. 2. Mole fractions of the fuels and main reaction products recorded during the oxidation of methane and ammonia in the flow tube reactor (Φ=1). Symbols: experiments (close symbols in panel a) are for methane-ammonia co-oxidation, open symbols are for neat methane oxidation). Lines: data computed with the model.

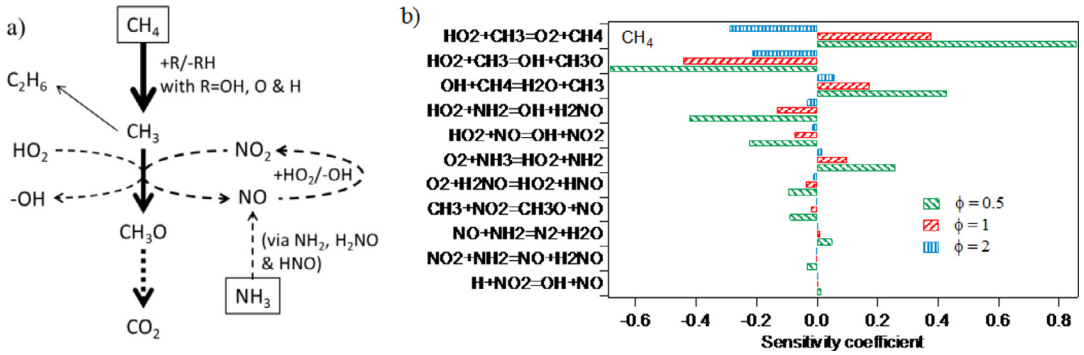

Fig. 3. a) Consumption pathways of methane and ammonia, and b) sensitivity analysis for methane mole fraction at variable Φ for ~1% CH_4 conversion. Sensitivity coefficients are normalized with respect to the value of $H+O_2=O+OH$ (not included).

during the co-oxidation of methane and ammonia, and their mutual interactions. Figure 3 presents a rate analysis for fuel consumption (Fig. 3a) and a sensitivity analysis for methane mole fraction (Fig. 3b) performed under JSR conditions (944 K, $\varphi = 0.5$, corresponding to conversions of 18% and 9% of methane and ammonia, respectively). Figure 4 displays a rate analysis for fuel consumption (Fig. 4b) and a sensitivity analysis for methane mole fraction (Fig. 4a) performed under FR conditions (~1560 K, $\varphi = 1$, and an abscissa of 46 cm (length from the tube inlet) corresponding to methane and ammonia conversions of ~50% and ~20%, respectively).

At low temperatures and under JSR conditions, the analysis shows that the consumption of methane starts with the classic H-atom abstraction reaction, $CH_4+OH=CH_3+H_2O$. The main consumption route of CH_3 is $CH_3+NO_2=CH_3O+NO$ (as in the case of the oxidation of methane doped with NO and NO_2 [22]), NO_2 coming from the reaction $NO+HO_2=NO_2+OH$. Minor channels are $CH_3+HO_2=CH_3O+OH$ and the recombination reaction forming ethane. Afterwards, the reaction

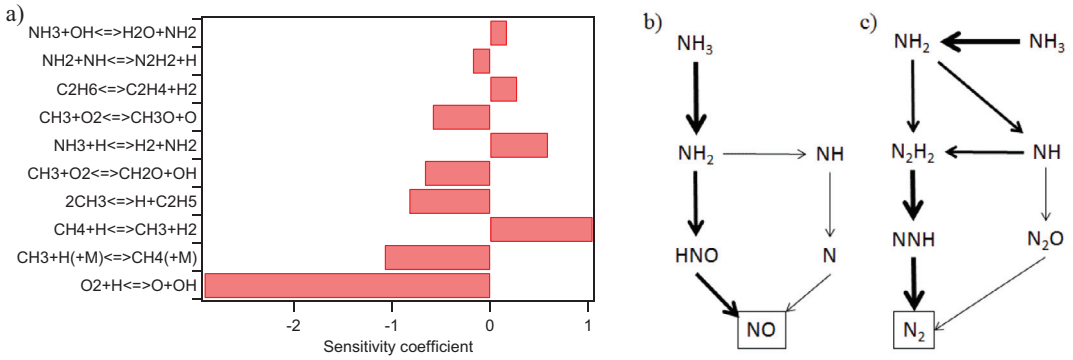

Fig. 4. a) Sensitivity diagram for methane under the FR conditions. b) and c) Formation routes to NO and N_2 ($T = 1560$ K, $\Phi = 1$, $x = 46$ cm (length from the tube inlet)). Arrow thickness is proportional to the reaction flux.

series leading to CO_2, via CH_3O, CH_2O, CHO, CO, is not directly affected by the presence of ammonia. The central role of the HO_2 radicals in converting CH_3 to CH_3O is noteworthy, through both direct reaction with CH_3 and indirectly by regenerating NO_2 from NO. The main sources of HO_2 radicals are the reactions $HCO+O_2=CO+HO_2$ and $H + O_2(+M)=HO_2(+M)$.

In these conditions, ammonia is mainly consumed by H-abstraction by HO_2, which is present in significant amounts at low temperatures. The high amounts of HO_2 also cause the termination of NH_2 radical, such as the reverse reaction prevails over the forward H-abstraction, and acts as a termination. This effect had already been noticed by Stagni et al. [7] in the oxidation of pure ammonia, although in this setup it does not affect reactivity to a significant extent (Fig. 3b) because of the presence of methane in higher amounts. NH_2 holds a key role in modifying the reactivity of pure methane: it reacts with NO and NO_2, and each of these two paths owns a branching and a terminating channel. The sensitivity analysis (Fig. 3b), carried out at different Φ for the same CH_4 conversion (1%), highlights the importance of H_2NO, formed by both branching channels and by NH_2 reaction with HO_2. H_2NO is then further oxidized to HNO and finally to NO (the chemistry of H_2NO is one of the biggest challenges in ammonia kinetics [21,32]). The interplay between NO_2 and NO is also evident in the sensitivity analysis, since NO_2 formation via $NO+HO_2$ enhances reactivity, and vice versa for its disappearance via its reaction with H. Indeed, NO_2 is the key molecule in sensitizing methane chemistry: the formation of the reactive methoxy radical (CH_3O) triggers the oxidation process of methane, as already shown in [22]. Therefore, the two reactions $CH_3+NO_2=CH_3O+NO$ and $NO+HO_2=NO_2+OH$ act as a catalytic cycle enhancing the consumption of methane. Conversely, with a richer mixture, the importance of ammonia chemistry becomes less and less important, and the lower amount of HO_2 stops the catalytic cycle. Thus, with increasing Φ, the usual CH_4 oxidation mechanism prevails, and sensitivity analysis shows that H-abstraction reactions and methyl conversion to methoxy govern the system reactivity.

Under FR conditions, there are fewer direct interactions between methane and nitrogenated species. Methane is still mainly consumed through H-abstractions by H, O and OH radicals. CH_3 radicals mainly react with O-atoms to yield CH_2O+H, i.e. bypassing CH_3O chemistry, crucial at lower temperatures. The second most important CH_3 reaction is the termination to ethane, and the third one is its interaction with NH forming CH_2NH+H. However, this does not have a significant impact on reactivity (Fig. 4a). Formaldehyde reacts following the usual sequence to give CO_2. CH_2NH chemistry is not discussed here as it is not determining. The sensitivity diagram in Fig. 4a shows that the reactivity is mainly governed by the chemistry of methane, whereas the impact of ammonia is minor, and limited to i) H-abstraction on ammonia itself, slowing down the reactivity since it subtracts active radicals for branching, and ii) N_2H_2 formation from NH_2 and NH, with consequent release of a H radical. Therefore, the oxidation paths of the two fuels is mostly governed by their independent interactions with the radical pool (H, O, OH).

As far as ammonia specific chemistry is concerned, the intermediate HNO plays a minor role under these high temperature conditions. The NH_2 radical mainly gives NH. It also reacts back to ammonia and leads to N_2H_2 by combination. N_2H_2 is converted into N_2, one of the major reaction products, through NNH. The NH radical mainly reacts with CH_3 yielding CH_2NH, while its second most important consumption route is to produce N_2H_2. It also yields N_2 via N_2O and NO, another major reaction product, via N. Rate of production analysis shows that N_2O mostly acts as an intermediate

species rather than as a final product, due to the high temperatures involved, causing its quick decomposition to N_2 and O. Anyway, the main NO formation pathway is still through HNO, which is formed from NH_2, although it is a minor consumption pathway for this last species.

Conclusions

In this work, the co-oxidation of methane and ammonia was experimentally and theoretically studied to investigate their mutual interactions in combustion processes. Experiments were performed in a jet-stirred reactor and in a newly developed flow tube reactor working up to ∼2000 K. Comparison of experimental data with simulations using a novel detailed kinetic model showed a satisfactory agreement for the reactivity and for the mole fractions of most reaction products. The kinetic analysis of the system shed light on the underlying causes of the NH_3 promoting effect, and on the major role played by NO in anticipating methane reactivity at low temperature. Although the effect of NO as a reactivity enhancer had been already established in previous works [22], it was observed in the present work that even as an intermediate species in the ammonia oxidation path, it affects methane oxidation to a major extent, shifting the reactivity onset by up to ∼100 K, especially in the leanest conditions. This effect is not present at higher temperatures where the reactivity is mainly governed by fuel H-abstractions by OH, O and H. In this case, as soon as methane reacts, the radical pool necessary to trigger ammonia oxidation becomes available, such as the reactivity onset of the two fuels occurs at the same temperature, and is slightly anticipated with respect to pure CH_4 mostly because of the higher amount of fuel.

Declaration of Competing Interest

The authors declare that they have no known competing financial interests or personal relationships that could have appeared to influence the work reported in this paper.

Acknowledgments

This work has received funding from the European Union H2020 (H2020-SPIRE-04-2016) under grant agreement n°723706.

Supplementary material

Supplementary material associated with this article can be found, in the online version, at doi:10.1016/j.proci.2020.07.061.

References

[1] D.P.B.T.B. Strik, A.M. Domnanovich, P. Holubar, *Process Biochem.* 41 (2006) 1235–1238. https://doi.org/10.1016/j.procbio.2005.12.008.
[2] R.O. Arazo, D.A.D. Genuino, M.D.G. de Luna, S.C. Capareda, *Sustain. Environ. Res.* 27 (2017) 7–14. https://doi.org/10.1016/j.serj.2016.11.010.
[3] H. Kobayashi, A. Hayakawa, K.D.K.A. Somarathne, E.C. Okafor, *Proc. Combust. Inst.* 37 (2019) 109–133. https://doi.org/10.1016/j.proci.2018.09.029.
[4] J. Ikäheimo, J. Kiviluoma, R. Weiss, H. Holttinen, *Int. J. Hydrog. Energy* 43 (2018) 17295–17308. https://doi.org/10.1016/j.ijhydene.2018.06.121.
[5] H. Xiao, A. Valera-Medina, P.J. Bowen, *Energy* 140 (2017) 125–135. https://doi.org/10.1016/j.energy.2017.08.077.
[6] A.J. Reiter, S.-.C. Kong, *Fuel* 90 (2011) 87–97. https://doi.org/10.1016/j.fuel.2010.07.055.
[7] A. Stagni, C. Cavallotti, S. Arunthanayothin, et al., *React. Chem. Eng.* 5 (2020) 696–711. https://doi.org/10.1039/C9RE00429G.
[8] A.A. Konnov, I.V. Dyakov, J.D. Ruyck, *Combust. Sci. Technol.* 178 (2006) 1143–1164. https://doi.org/10.1080/00102200500296788.
[9] B. Li, Y. He, Z. Li, A.A. Konnov, *Combust. Flame* 160 (2013) 40–46. https://doi.org/10.1016/j.combustflame.2012.10.003.
[10] B.A. Williams, J.W. Fleming, *Combust. Flame* 110 (1997) 1–13. https://doi.org/10.1016/S0010-2180(97)00063-1.
[11] I. Rahinov, A. Goldman, S. Cheskis, *Combust. Flame* 145 (2006) 105–116. https://doi.org/10.1016/j.combustflame.2005.11.004.
[12] A. Garo, C. Hilaire, D. Puechberty, *Combust. Sci. Technol.* 86 (1992) 87–103. https://doi.org/10.1080/00102209208947189.
[13] X. Han, Z. Wang, M. Costa, Z. Sun, Y. He, K. Cen, *Combust. Flame* 206 (2019) 214–226. https://doi.org/10.1016/j.combustflame.2019.05.003.
[14] E.C. Okafor, Y. Naito, S. Colson, et al., *Combust. Flame* 204 (2019) 162–175. https://doi.org/10.1016/j.combustflame.2019.03.008.
[15] T. Mendiara, P. Glarborg, *Combust. Flame* 156 (2009) 1937–1949. https://doi.org/10.1016/j.combustflame.2009.07.006.
[16] V.J. Wargadalam, G. Löffler, F. Winter, H. Hofbauer, *Combust. Flame* 120 (2000) 465–478. https://doi.org/10.1016/S0010-2180(99)00107-8.
[17] M. Barbas, M. Costa, S. Vranckx, R. Fernandes, Experimental and kinetic modeling study of CO and NO formation under oxy-fuel conditions, in: 2015: pp. 16–20.
[18] O. Mathieu, M.M. Kopp, E.L. Petersen, *Proc. Combust. Inst.* 34 (2013) 3211–3218. https://doi.org/10.1016/j.proci.2012.05.008.
[19] S. Liu, C. Zou, Y. Song, S. Cheng, Q. Lin, *Energy* 175 (2019) 250–258. https://doi.org/10.1016/j.energy.2019.03.040.
[20] K.P. Shrestha, L. Seidel, T. Zeuch, F. Mauss, *Energy Fuels* 32 (2018) 10202–10217. https://doi.org/10.1021/acs.energyfuels.8b01056.
[21] P. Glarborg, J.A. Miller, B. Ruscic, S.J. Klippenstein, *Prog. Energy Combust. Sci.* 67 (2018) 31–68. https://doi.org/10.1016/j.pecs.2018.01.002.

[22] Y. Song, L. Marrodán, N. Vin, et al., *Proc. Combust. Inst.* 37 (2019) 667–675. https://doi.org/10.1016/j.proci.2018.06.115.
[23] L. Marrodán, Y. Song, M. Lubrano Lavadera, et al., *Energy Fuels* 33 (2019) 5655–5663. https://doi.org/10.1021/acs.energyfuels.9b00536.
[24] M. Pelucchi, S. Namysl, E. Ranzi, et al., *Proc. Combust. Inst.* 37 (2019) 389–397. https://doi.org/10.1016/j.proci.2018.07.087.
[25] C. Bahrini, O. Herbinet, P.-.A. Glaude, C. Schoemaecker, C. Fittschen, F. Battin-Leclerc, *J. Am. Chem. Soc.* 134 (2012) 11944–11947. https://doi.org/10.1021/ja305200h.
[26] L. Marrodán, Y. Song, O. Herbinet, et al., *Chem. Phys. Lett.* 719 (2019) 22–26. https://doi.org/10.1016/j.cplett.2019.01.038.
[27] E. Ranzi, A. Frassoldati, R. Grana, et al., *Prog. Energy Combust. Sci.* 38 (2012) 468–501. https://doi.org/10.1016/j.pecs.2012.03.004.
[28] W.K. Metcalfe, S.M. Burke, S.S. Ahmed, H.J. Curran, *Int. J. Chem. Kinet.* 45 (2013) 638–675. https://doi.org/10.1002/kin.20802.
[29] S.M. Burke, U. Burke, R. Mc Donagh, et al., *Combust. Flame* 162 (2015) 296–314. https://doi.org/10.1016/j.combustflame.2014.07.032.
[30] A. Burcat, B. Ruscic, *Chemistry, T.-I.I. of Tech, Third Millenium Ideal Gas and Condensed Phase Thermochemical Database for Combustion (with update from active thermochemical tables)*, Argonne National Lab. (ANL), Argonne, ILUnited States, 2005 https://doi.org/10.2172/925269.
[31] M. Lubrano Lavadera, Y. Song, P. Sabia, et al., *Energy Fuels* 32 (2018) 10088–10099. https://doi.org/10.1021/acs.energyfuels.8b00967.
[32] A. Stagni, Y. Song, L.A. Vandewalle, et al., *Chem. Eng. J.* 385 (2020) 123401. https://doi.org/10.1016/j.cej.2019.123401.